Nonstationarity in Southern Hemisphere Climate Variability Associated with the Seasonal Breakdown of the Stratospheric Polar Vortex

NICHOLAS J. BYRNE AND THEODORE G. SHEPHERD

Department of Meteorology, University of Reading, Reading, United Kingdom

TIM WOOLLINGS

Atmospheric, Oceanic and Planetary Physics, University of Oxford, Oxford, United Kingdom

R. ALAN PLUMB

Department of Earth, Atmospheric and Planetary Sciences, Massachusetts Institute of Technology, Cambridge, Massachusetts

(Manuscript received 15 February 2017, in final form 17 May 2017)

ABSTRACT

Statistical models of climate generally regard climate variability as anomalies about a climatological seasonal cycle, which are treated as a stationary stochastic process plus a long-term seasonally dependent trend. However, the climate system has deterministic aspects apart from the climatological seasonal cycle and long-term trends, and the assumption of stationary statistics is only an approximation. The variability of the Southern Hemisphere zonal-mean circulation in the period encompassing late spring and summer is an important climate phenomenon and has been the subject of numerous studies. It is shown here, using reanalysis data, that this variability is rendered highly nonstationary by the organizing influence of the seasonal breakdown of the stratospheric polar vortex, which breaks time symmetry. It is argued that the zonal-mean tropospheric circulation variability during this period is best viewed as interannual variability in the transition between the springtime and summertime regimes induced by variability in the vortex breakdown. In particular, the apparent long-term poleward jet shift during the early-summer season can be more simply understood as a delay in the equatorward shift associated with this regime transition. The implications of such a perspective for various open questions are discussed.

1. Introduction

The interval encompassing late spring and summer represents a time frame of uncommon interest for Southern Hemisphere (SH) climate variability. The stratosphere–troposphere coupling evident in the southern annular mode (SAM) pattern of variability maximizes during this period (Thompson and Wallace 2000). There is a concomitant increase in SAM persistence time scales, which suggests potential for skillful seasonal forecasting (Baldwin et al. 2003; Kidston et al. 2015). The teleconnection between El Niño–Southern Oscillation (ENSO) and SH high-latitude climate also maximizes during this period (Seager et al. 2003; L'Heureux and Thompson 2006). Finally, the largest changes in the SH circulation over the past half-century have occurred during the summer season (Fogt et al. 2009). Modeling studies have implicated stratospheric ozone depletion as the most likely driver of these changes (see Thompson et al. 2011, and references therein), and indeed they represent the only observed circulation changes so far attributable to human influence (IPCC 2013). Despite much study of these various phenomena, the responsible mechanisms have yet to be conclusively identified.

In all these studies, the approach has been to regard the intraseasonal and interannual variability, and the long-term changes, as anomalies about the climatological seasonal cycle. The statistical methods used then generally treat those anomalies in the usual way as a stationary stochastic process (i.e., with statistics that are

Corresponding author: Nicholas J. Byrne, n.byrne@pgr.reading.ac.uk

DOI: 10.1175/JCLI-D-17-0097.1

invariant under time translation) plus a long-term seasonally dependent trend. However, Byrne et al. (2016) have recently argued that the variability of the SH zonal-mean circulation should not be treated as a stationary stochastic process because of the presence of nonstationary interannual variability, which exhibits a strong 2-yr peak. The effect is most pronounced between late spring and early summer. These two features point to the role of the stratosphere.

Black and McDaniel (2007) suggested that the annual spring breakdown of the stratospheric polar vortex acts as an organizing influence on the variability of the SH zonal-mean circulation, although they found only a weak influence on the zonal-mean tropospheric circulation. More recently, Sun et al. (2014) used both reanalyses and a hierarchy of models to argue that the long-term changes in the vortex breakdown dates were responsible for the long-term changes in the zonal-mean tropospheric circulation. That the vortex breakdown event can act as an organizing influence on tropospheric variability implies that a stationary model of tropospheric variability is suspect, given that the vortex breakdown is a singular event within the seasonal cycle that breaks time symmetry. Moreover, the breakdown event itself is known to be affected by nonstationary sources of variability such as the quasi-biennial oscillation (QBO) and solar cycle (e.g., Anstey and Shepherd 2014). Rather than viewing variability (and long-term changes) of SH late spring and early summer circulation as anomalies to a climatological seasonal cycle, it may be more useful to regard it as variability in the seasonal transition between spring and summer, which is organized around the date of the stratospheric vortex breakdown. The purpose of this paper is to explore the implications of this perspective for the various topics mentioned earlier.

The plan of the paper is as follows. Section 2 gives full details of the data and methods used in this paper. Section 3 presents reanalysis evidence for our proposed perspective on circulation variability. Section 4 considers the implications of this perspective for several previous results in the literature. We then conclude the paper in section 5 with a summary of our results and a discussion of possible future work.

2. Data and methods

The basic data input for our study is 4-times daily zonal wind data from the ERA-Interim dataset (Dee et al. 2011) for the period 1 June 1979–31 May 2016. This period encompasses 37 yr in total in the SH. Data were available on an N128 Gaussian grid and on 37 pressure levels (1000–1 hPa). Before analyzing the data we first processed it by forming a daily and zonal average of the data. This processed data formed the input for all of our subsequent analysis. We define a climatology of our data as the long-term daily average that is subsequently smoothed by retaining the first six Fourier harmonics (Black et al. 2006; Black and McDaniel 2007). We define a daily jet-latitude index by mass-weighting our data, vertically averaging it between 1000 and 250 hPa, and subsequently computing the latitude of the maximum daily value of this average between 0° and 90°S. We identify the date of the vortex breakdown as the final time that the zonal-mean daily mean zonal wind at 60°S drops below $10\,\mathrm{m\,s^{-1}}$; we apply this criterion to running 5-day averages at 50 hPa (Black and McDaniel 2007). We define early and late breakdown events as the 18 earliest and latest breakdown events (separated by one median event, 1993).

We define a SAM index for each pressure level of our data in a similar manner to Simpson et al. (2011). First we compute daily anomaly data by removing a daily climatology. Next we perform an empirical orthogonal function (EOF) analysis between 20° and 90°S and at each individual level; we weight our data to account for the decrease in area toward the pole (North et al. 1982). Finally we define our SAM index as the normalized principal component time series that results from our EOF analysis. To compute our SAM autocorrelation function *e*-folding time scale we follow the method of Mudryk and Kushner (2011) (see also Simpson et al. 2011). We obtained our time series for effective equivalent stratospheric chlorine (EESC) from the Goddard Space Flight Center automailer service (https://acd-ext.gsfc.nasa.gov/Data_services/automailer/). Our EESC time series was generated by specifying a mean age of air of 5.5 yr (Newman et al. 2006), which is appropriate for the ozone hole. Linear trends and EESC regression values are calculated for each day of the year after the daily data are first smoothed using a Gaussian window with a 7-day half width (Sun et al. 2014).

Variations in ENSO are defined using the Niño-3.4 sea surface temperature index obtained from the NOAA/Earth System Research Laboratory website (www.esrl.noaa.gov/psd/gcos_wgsp/Timeseries/Nino34). This index was detrended and standardized using the same time period as our reanalysis data prior to analysis. ENSO episodes are defined using the oceanic Niño index (ONI), according to the NOAA Climate Prediction Center definition (www.cpc.ncep.noaa.gov/products/analysis_monitoring/ensostuff/ensoyears.shtml). Specifically, El Niño episodes are defined as five consecutive overlapping 3-month periods at or above the +0.5°C anomaly relative to the base period chosen for the ONI,

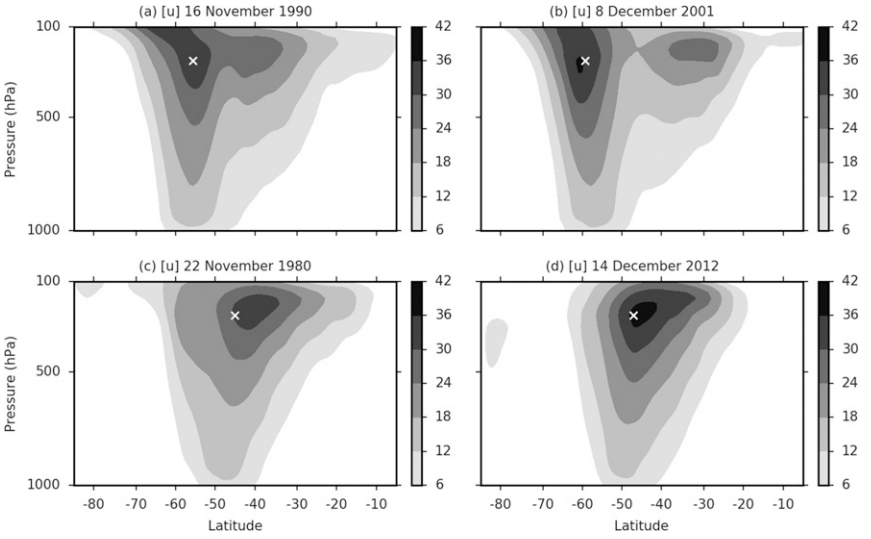

FIG. 1. Daily mean snapshots of $[u]$ ($\mathrm{m\,s^{-1}}$). Values below $6\,\mathrm{m\,s^{-1}}$ have been masked for presentation purposes. Crosses denote the daily latitude of the jet according to our jet-latitude index.

while La Niña episodes are defined as five consecutive overlapping 3-month periods below the −0.5°C anomaly relative to the base period. Periods where neither of these criteria are met are referred to as neutral episodes. We do not distinguish between the strength of ENSO episodes.

3. Composite analysis

a. Climatology

We employ zonal-mean zonal wind $[u]$, where the square brackets denote the zonal mean, as a measure of the large-scale extratropical circulation. From late October to the following May, the dominant feature in $[u]$ in the SH troposphere is an approximately equivalent barotropic jet in the extratropics that extends to the surface (e.g., Hartmann and Lo 1998). Snapshots of this structure, for the months of November and December, are shown in Fig. 1 for reference. This structure is frequently referred to as the eddy-driven jet, and hereafter we refer to it simply as the jet. Definitions for the daily latitude of the jet commonly exploit either its lack of vertical tilt (equivalent barotropic property) or the strength of the near-surface winds in the region of the jet (surface extension property). We make use of the equivalent barotropic property and define the latitude of the jet as the latitude of the maximum value of the mass-weighted vertical average of $[u]$ between 1000 and 250 hPa. For the remainder of the paper we denote this vertical average as $\langle [u] \rangle$.

Figure 2 shows the climatological seasonal cycle of $\langle [u] \rangle$ from the middle of October (mid-to-late spring) to the middle of January (midsummer). In a climatological sense, the jet is seen to exist at a more poleward latitude in mid-to-late spring compared to early summer. This description also appears valid in a more deterministic sense: inspection of individual years reveals that the picture of a more poleward jet in mid-to-late spring relative to early summer offers a fair description of 33 out of the 37 yr considered. The years where this description does not appear appropriate include the spring seasons of 1988 and 2002 along with, to a lesser extent, 1996 and 2007. The climatological plot suggests an equatorward transition between the two states from early November to late December, with a change in jet latitude on the order of 5° over a time scale on the order of 50 days. There is also a

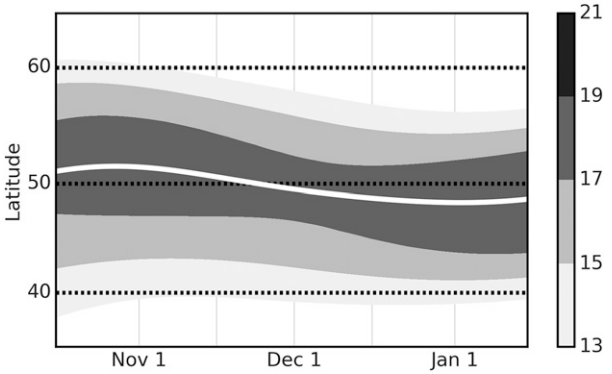

FIG. 2. Climatology of $<[u]>$ (shading; $\mathrm{m\,s^{-1}}$) and jet-latitude index (white line) from 16 October to 15 January.

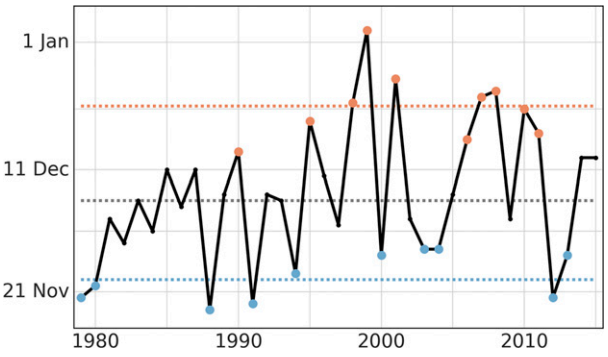

FIG. 3. Time series of the annual SH stratospheric vortex breakdown date (solid line). The median date is 6 December (gray dashed line). The extreme late (red) and extreme early (blue) breakdown years (dots) along with the median dates for these years (dashed lines) are also plotted. The breakdown date has been subject to a long-term trend that has been attributed to SH ozone depletion (see Thompson et al. 2011). [Figure is updated from Fig. 1 of Black and McDaniel (2007).]

hint of a weakening in the strength of the jet during the transition period, as evidenced by the narrowing of the highest contour level. From inspection of individual years there does appear to be some evidence to support this notion of a weakening during the transition period, with some years exhibiting an occasional loss of jet coherence resulting in a relatively broad band of westerlies and weaker surface winds. However, this phenomenon appears to be limited to at most 8 out of the 37 yr considered, and so for purposes of simplicity, in the remainder of this study we consider the transition between spring and summer to reflect purely a shift in jet latitude.

A feature that emerges more clearly from inspection of individual years is that the timing of this transition in jet latitude appears to exhibit significant interannual variability. Particular examples of this variability can be seen in Fig. 1; Figs. 1a,b represent snapshots of the jet taken from years where the seasonal transition has yet to occur, and Figs. 1c,d represent snapshots of the jet in years where the seasonal transition has already taken place. This variability in the timing of the seasonal transition is highlighted in greater detail in the next subsection.

b. *Breakdown date composites*

To quantify the organizing influence of the breakdown of the stratospheric polar vortex on the variability of the SH circulation, Black and McDaniel (2007) introduced composite plots of the zonal-mean circulation centered around the breakdown date for each year. The breakdown date is subject to substantial interannual variability (see Fig. 3 for a measure of this variability), and so composite plots were used as a means of isolating the recurring features of the circulation associated with the breakdown event. In several of these composites, circulation anomalies about the climatological seasonal cycle were used as the primary data input (hereafter, unless otherwise stated, we refer to anomalies about a climatological seasonal cycle simply as anomalies). Figure 4 is an example of such an anomaly composite; it has been vertically integrated to allow for comparison across latitude bands. At high latitudes in the weeks either side of the breakdown event there is a hint of an organizing influence, as suggested by the sharp change in sign of the anomalies around lag 0 day. However, the anomaly magnitudes are relatively small and cannot clearly be distinguished from natural variability, consistent with Black and McDaniel's (2007) finding of a weak influence on the troposphere.

We now construct composite plots of (i) breakdown events that occur either prior to or after the median climatological vortex breakdown event and (ii) the 10 earliest and 10 latest breakdown events, which represent respectively the lower and upper quartiles of breakdown dates. Hereafter we refer to events prior to and after the vortex breakdown as early and late events and to the

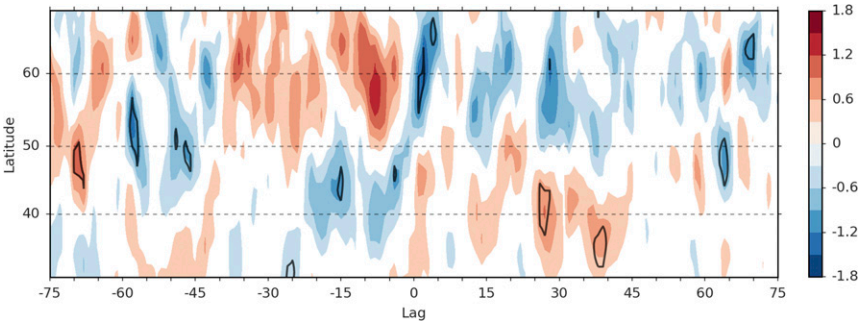

FIG. 4. Composite plot of $<[u]>$ anomalies (shading; m s^{-1}) centered about the stratospheric vortex breakdown date. Black contours indicate anomalies that are significant at the 5% level, based on the two-sided one-sample Student's t test for a reference mean value of zero. Values between -0.3 and 0.3 m s^{-1} have been masked for presentation purposes.

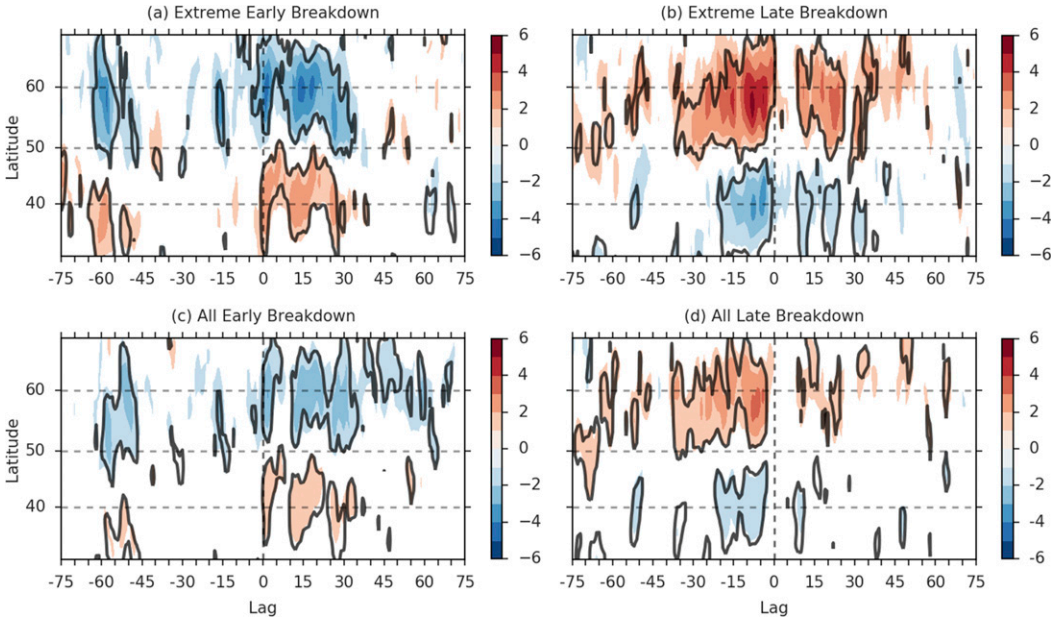

FIG. 5. Composite plots of $\langle [u] \rangle$ anomalies (shading; m s^{-1}) relative to the actual stratospheric vortex breakdown date for (a) extreme early years, (b) extreme late years, (c) all early years, and (d) all late years. Black contours indicate anomalies that are significant at the 5% level, based on the one-sided one-sample Student's t test for a reference mean value of zero. Values between -1 and 1 m s^{-1} have been masked for presentation purposes.

lower and upper quartiles as extreme early and extreme late events. The plots for all of these subgroups are shown in Fig. 5, and from inspection, it is immediately clear that they all contain very different anomaly patterns from that shown in Fig. 4. The strengths are also very different—note the very different color scale—and clearly distinguishable from natural variability. Early breakdown years are seen to be associated with persistent high-latitude negative anomalies that are particularly prominent between lags 0 and +30 days. Late breakdown years are seen to be associated with persistent high-latitude positive anomalies that are particularly prominent between lags −40 and 0 days and to a lesser extent between lags +10 and +30 days. Opposite-signed anomalies are seen in midlatitudes. Anomaly magnitudes for both early and late breakdown years are seen to be enhanced for extreme breakdown events, which offer an illustration of how different the actual circulation can be compared to that predicted by the climatology around the time of the vortex breakdown date. Figure 4 can be approximately recovered by combining Figs. 5c and 5d, but the dilution of the two very different signals means that the structure can no longer be distinguished from the noise. This distinct difference between anomaly patterns for early and late breakdown events is prima facie evidence for treating anomalies around the time of the vortex breakdown as a nonstationary process.

That the anomalies around the time of the vortex breakdown should be modeled as a nonstationary stochastic process implies that the physical relevance of a climatological seasonal cycle is suspect. To explore this issue further, we compute early and late composites of $\langle [u] \rangle$ (i.e., we do not remove a climatological seasonal cycle prior to computation of the composite plots; see Figs. 6a,c). In both of these plots the jet transitions equatorward, commencing several weeks prior to the vortex breakdown date and concluding shortly afterward.[1] Also evident is the apparent tendency for early breakdown events to be associated with a more equatorward jet transition. Rather than viewing the climatological seasonal cycle as a relatively slow equatorward transition of the jet, the composite plots suggest that it should instead be interpreted as an average of yearly equatorward jet transitions, organized about the vortex breakdown date, which diffuses the sharpness of the transition seen in individual years. This interpretation is further supported by calculating a climatological seasonal cycle for early and late breakdown years separately (see Figs. 6b,d). The two climatological cycles are seen to be quite different,

[1] It should be noted that for individual years there will be day-to-day variability superimposed on this transition. "Wiggles" in our jet-latitude index should not necessarily be interpreted as coherent jet variability and may be an artifact of our limited sample size.

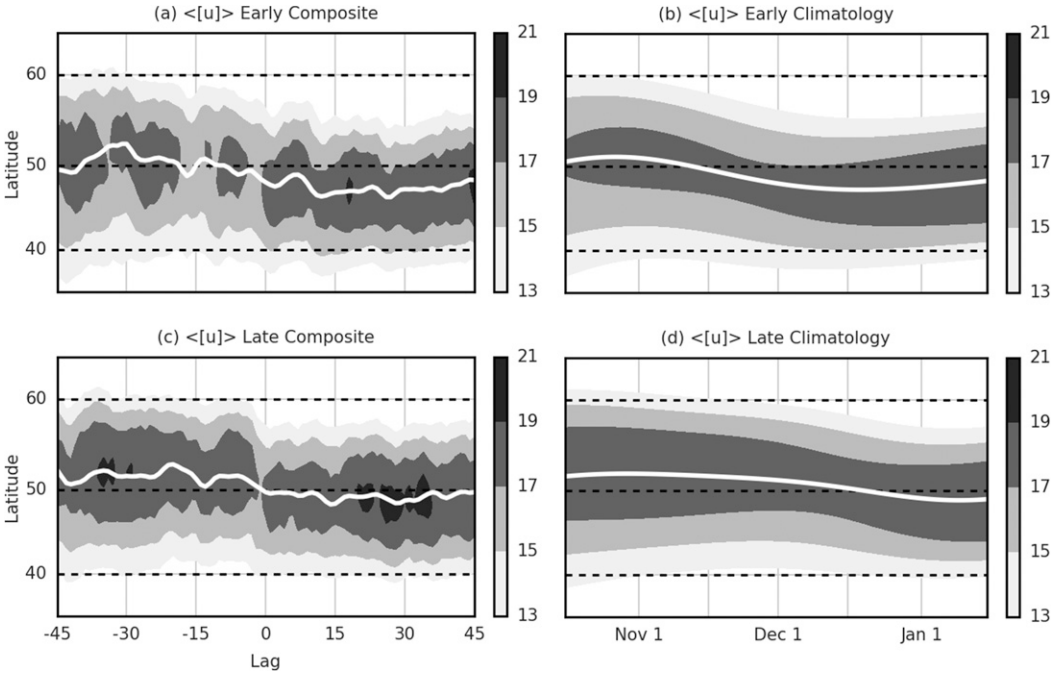

FIG. 6. Composite plots of $\langle [u] \rangle$ (shading; m s^{-1}) and jet-latitude index (white line), centered about the stratospheric vortex breakdown date, for (a) all early years and (c) all late years. Jet-latitude index has been smoothed with a binomial filter of order 4 for presentation purposes. Climatology of $\langle [u] \rangle$ (shading; m s^{-1}) and jet-latitude index (white line) from 16 October to 15 January for (b) all early years and (d) all late years. Values below 13 m s^{-1} have been masked for presentation purposes.

consistent with an organizing influence from the vortex breakdown event. Such an organizing influence of the vortex breakdown on the jet has recently been documented across a hierarchy of models by Sun et al. (2014). These authors also noted that early and late vortex breakdown events appeared to exhibit somewhat distinct evolutions, beyond a simple translation in time of the breakdown dates. They hypothesized that both the timing and type of breakdown event are important for characterizing the organizing influence on the troposphere, consistent with the results from our jet composites.

To try to understand the impact of variations in the timing of the breakdown date on anomaly composites, we introduce a schematic of the seasonal jet transition in Fig. 7. This schematic is motivated by the results of our composite plots in Fig. 6 and neglects any potential evolutionary differences between early and late breakdown events, in an attempt to isolate the influence of breakdown date variability. We also restrict the schematic to extreme years, as these are the years where we expect the impact from variations in the timing of the event to be most pronounced.

In extreme early years in our schematic, as a result of the earlier circulation transition, circulation anomalies can be expected to exhibit a persistent dipolar structure that is negative on the poleward flank of our jet-latitude index and positive on the equatorward flank (Fig. 7c). In extreme late years, we can expect the opposite behavior to emerge (Fig. 7d). As a result of the stronger meridional gradients on the poleward flank of our idealized jet profile (Fig. 7b), the circulation anomalies are larger on the poleward flank than on the equatorward flank for a given latitude shift. Furthermore, in the distribution of early years in our schematic, we find that anomalies emerge from about 15 days prior to almost 30 days after the vortex breakdown date of that year. In the distribution of late years, we note that anomalies exist from about 50 to 5 days prior to the vortex breakdown date of that year. In the schematic, we see that very different anomaly structures are expected for early and late breakdown events; in this simplified setting, we can attribute the different anomaly structures to the differences in the date of the circulation transition for each individual year. We also see that the anomalies can be characterized by very long persistence time scales, even though the transition is itself a comparatively rapid event. This has implications for the understanding of SAM persistence time scales, as discussed in section 4a.

The predictions of our schematic are in good qualitative agreement with the anomaly patterns in Fig. 5. In particular, the sign and temporal structure of the anomalies share a close correspondence. We also note that anomaly

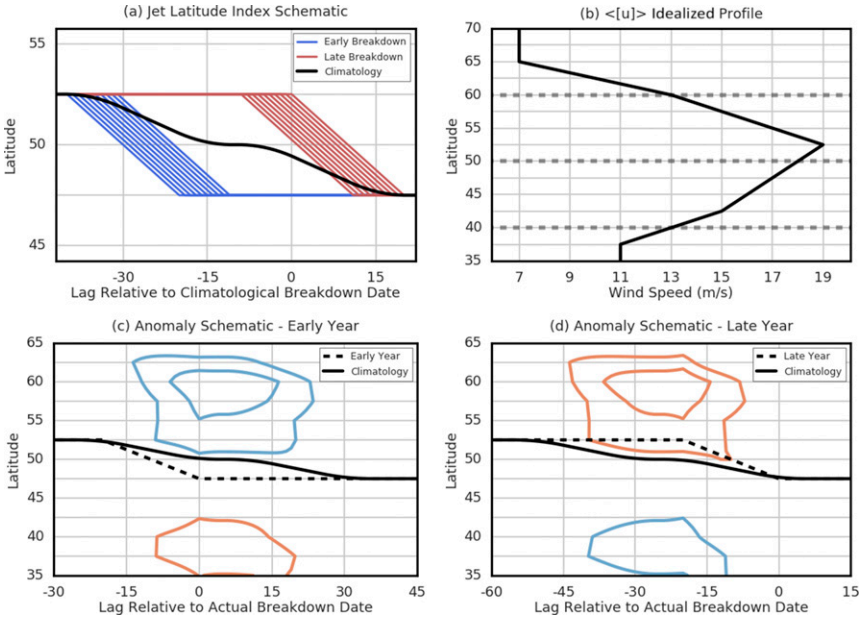

FIG. 7. (a) Schematic for jet-latitude index. Individual lines represent an idealized jet-latitude index for individual years. Extreme early breakdown years are defined as years where the vortex breakdown occurs between 11 and 20 days prior to the climatological vortex breakdown date (we consider a uniform distribution between lags −11 and −20 days) and extreme late years are defined in a similar manner. For each year we imagine our jet to exist at a fixed latitude until 20 days prior to the vortex breakdown date of that year. At 20 days prior to the breakdown date we then imagine it to transition equatorward in a linear fashion and, subsequent to this breakdown date, to again persist at a fixed, relatively more equatorward, latitude. The transition time scale and breakdown dates are taken as representative of the reanalysis data (see Figs. 3 and 6). We form a climatology by averaging the jet behavior across all years (i.e., by averaging the blue and red lines). Schematic for zonal-mean zonal wind anomalies for (c) early and (d) late years. The schematic in (c),(d) is an extension of (a) by also incorporating an idealized profile for $\langle [u] \rangle$ [see (b)]. For each event in (a), we align the maximum value in the idealized jet profile with the location of the jet-latitude index. We construct a climatology for $\langle [u] \rangle$ by averaging over all breakdown events. We then plot the jet-latitude index for breakdown events that are 15 days earlier and 15 days later than the climatological breakdown date (dashed lines), along with the difference between $\langle [u] \rangle$ for these breakdown events and the climatology of $\langle [u] \rangle$ (contours). The contour interval is 1 m s^{-1}. Red and blue contours indicate positive and negative values, respectively; the zero contour is not plotted.

amplitudes decrease somewhat when all years are considered, consistent with the idea that extreme variability in the breakdown date is associated with large anomalies about the climatological seasonal cycle. Not all features of the anomaly composites are predicted by our schematic; the reemergence in extreme late years of persistent positive anomalies, from about lag +10 day, is perhaps the most obvious example. This suggests that this feature is associated with differences in the type of breakdown event. Inspection of individual years reveals that the persistence of positive anomalies beyond the breakdown date appears restricted to a relatively small subset of exceptionally late breakdown years—the five latest breakdown years along with the summers of 2011/12 and 2015/16 (we note the disappearance of this feature when all late years are considered as quantitative evidence of this statement). These exceptionally late years appear to be associated with a reduced equatorward jet transition around the vortex breakdown date and, consequently, a more poleward jet in January. Thus, it appears likely that a combination of both the timing and type of breakdown is necessary to account fully for circulation anomalies around the vortex breakdown, as argued by Sun et al. (2014). Nevertheless, we derive some confidence from the fact that our schematic appears consistent with the preponderance of features seen in the anomaly composites.

The combined evidence of the composite plots, climatologies, and schematic leads us to propose that during late spring and early summer, zonal-mean tropospheric SH circulation variability is most naturally viewed as

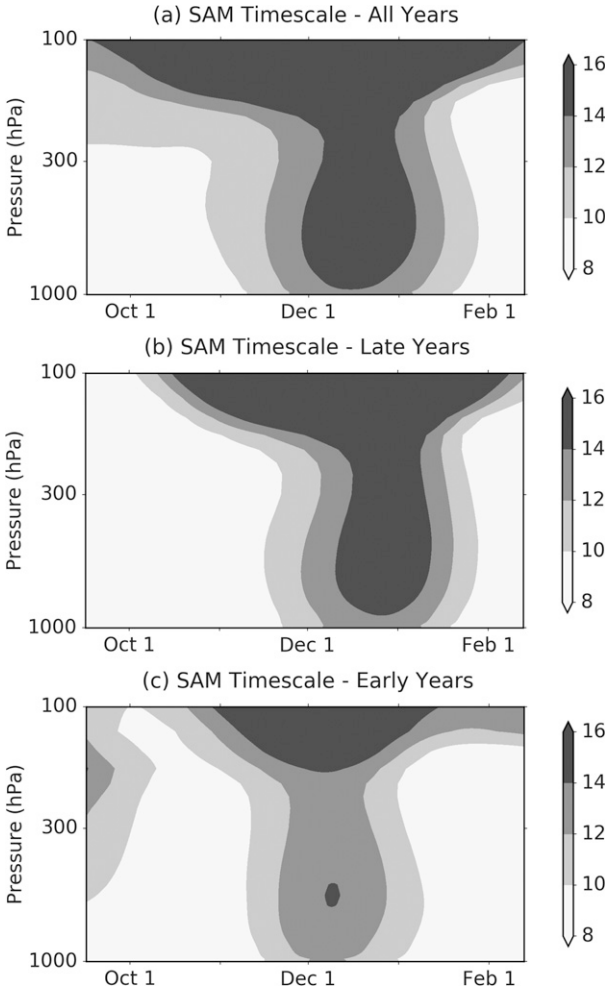

FIG. 8. SAM autocorrelation function *e*-folding time scale, as a function of day of the year and pressure level, for (a) all years, (b) all late years, and (c) all early years with 2002 excluded. The year 2002 is excluded in (c) as the austral spring of 2002 was unique for the occurrence of the only SH sudden stratospheric warming in the observational record, which was associated with a large amplitude disturbance in the tropospheric SAM index (see Fig. 7 of Thompson et al. 2005). Inclusion of 2002 does not qualitatively change our conclusions. [Figure is analogous to Fig. 1 of Baldwin et al. (2003).]

variability in the seasonal transition of the jet and that this transition is organized about the date of the breakdown of the stratospheric vortex. In the next section we consider the implications of this perspective for the various topics mentioned in the introduction of this paper.

4. Applications

a. Southern annular mode persistence time scales

A peculiar property of the large-scale extratropical SH circulation between November and January is that anomalies (as measured by the SAM index) appear to persist for longer than at other times of the year (Baldwin et al. 2003). Previous work has implicated stratospheric variability in this increase in tropospheric persistence time scales (e.g., Baldwin et al. 2003; Gerber et al. 2010), and this feature has generated interest as indicating a potential time of year where skillful long-range forecasts may be possible (see Kidston et al. 2015, and references therein). Usually the calculation is performed using zonal-mean geopotential height anomalies; however, balance considerations associated with the large-scale circulation (e.g., McIntyre 2015) suggest that this is also likely to be a feature of the zonal-mean zonal wind field. Figure 8a represents evidence in favor of this statement; it has been computed using zonal-mean zonal wind anomalies rather than geopotential height. The temporal and structural similarity between Fig. 8a and the earlier calculation of Baldwin et al. (2003) suggests that both plots are isolating the same feature of the circulation and that we can use zonal-mean zonal wind time scales as a proxy for geopotential height. The benefit of this transformation is that we can directly employ the results of the previous section to further our understanding of why this increased persistence feature emerges.

A complicating factor in applying our results is that the computational procedure for constructing Fig. 8 is somewhat involved (see appendix A of Mudryk and Kushner 2011). Nevertheless, a key component of the calculation involves projecting circulation anomalies onto a leading EOF structure. Figure 9 represents the leading EOF for $\langle [u] \rangle$ between 20° and 90°S.[2] The EOF is plotted in meters per second to illustrate typical anomaly magnitudes associated with one standard deviation of the SAM index. Comparison of this structure with the anomaly patterns in Fig. 5 reveals a close correspondence, and suggests that the composite anomalies are of the correct amplitude to provide a substantial contribution to the SAM index. This motivates the following interpretation for the increased SAM time scales between November and January: variability in the seasonal transition of the jet associated with variability in the date of the breakdown of the stratospheric vortex.

As evidence in favor of this interpretation, several recent modeling studies (e.g., Simpson et al. 2011;

[2] The leading EOF for $\langle [u] \rangle$ is closely associated with the leading EOF for $[u]$ at each level in the troposphere, as a result of the equivalent barotropic property of the jet. The SAM index at each level in the troposphere has a temporal correlation >0.95 with the SAM index formed using $\langle [u] \rangle$, based on a 37-yr daily time series.

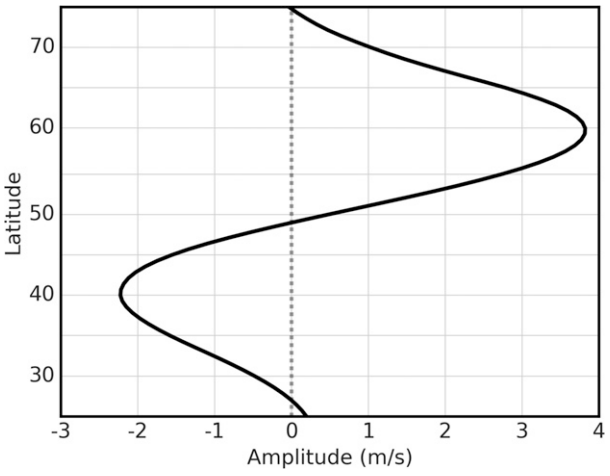

FIG. 9. Leading EOF of $\langle [u] \rangle$ (m s^{-1}) between 20° and 90°S.

Kim and Reichler 2016) have highlighted an important role for zonal-mean stratospheric variability in lengthening tropospheric SAM time scales. Furthermore, when years with similar vortex breakdown dates are grouped together, the period of long time scales in the troposphere is seen to narrow (cf. Fig. 8b and Fig. 8c with Fig. 8a). Finally, as an alternative means of quantifying the influence of interannual variability in the vortex breakdown date on tropospheric jet variability, we have developed a linear predictor model for the November–December mean jet latitude, using the date of the vortex breakdown as our predictor (see appendix A; $r \approx 0.73$). The relative success of this simple linear model is further evidence of the substantial organizing influence of the vortex breakdown event on the jet at this time of year. The combination of all these results leads us to conclude that the increase in SAM time scales between November and January can be largely interpreted as variability in the seasonal transition of the jet. This interpretation supports the idea that long-range skill in the prediction of the latitude of the tropospheric jet is possible at this time of year (see also Baldwin et al. 2003), although the source of such skill is attributed to the organizing influence of the stratospheric vortex breakdown rather than to enhanced persistence of SAM variability.

b. Southern Hemisphere high-latitude climate change

The positive trend of high-latitude circulation anomalies in austral summer has been a well-documented feature of the satellite era; it has been largely attributed to stratospheric ozone depletion (see Thompson et al. 2011, and references therein). This positive trend is commonly diagnosed using monthly mean geopotential height anomalies and has been interpreted as a poleward shift of the midlatitude jet. Here we perform a related calculation and diagnose decadal linear trends in $\langle [u] \rangle$ (see Fig. 10a). To confirm the qualitative robustness of the features of this plot to the potentially compensating effect of an ozone recovery since 2000 (Solomon et al. 2016), we have also performed a regression analysis against EESC (see Fig. 10b). In Fig. 10, the plotted contours are largely representative of regions that are statistically significant at the 5% level, and it is clear that they both share very similar features. As an alternative means of quantifying the significance of these features, we have also plotted the long-term means and standard errors for $\langle [u] \rangle$ for both the ozone depletion and ozone recovery eras (see Fig. 11).

Inspection of Figs. 10 and 11 reveals that there appear to be at least two distinct components to high-latitude changes in $\langle [u] \rangle$. Of primary interest to the present

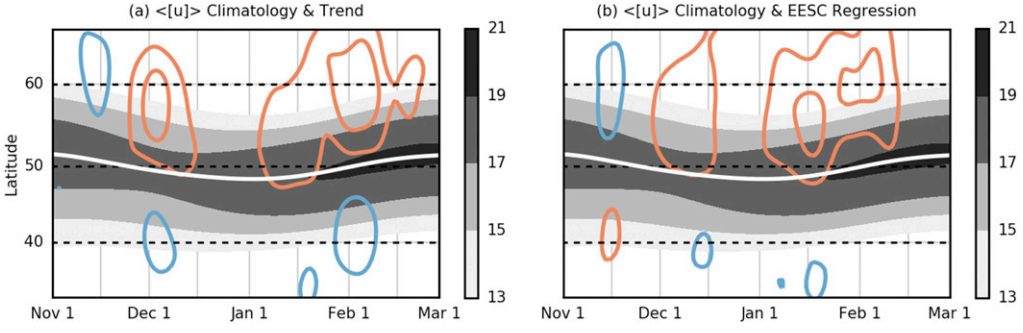

FIG. 10. (a) Climatology (shading; m s^{-1}) and linear trend (contours; m s^{-1} decade^{-1}) for $\langle [u] \rangle$ (m s^{-1}), along with jet-latitude index (white line), from 1 November to 1 March. Contour interval is 0.6 m s^{-1} decade^{-1}, and negative trends are indicated by blue contours and positive trends by red contours; the zero contour is not plotted. (b) As in (a), but with EESC regression values (contours). Contour interval is now 1 m s^{-1} decade^{-1}; we display trends in these units by scaling meters per second per pptv by the total change in EESC across the 1980s, a decade where EESC increased approximately linearly.

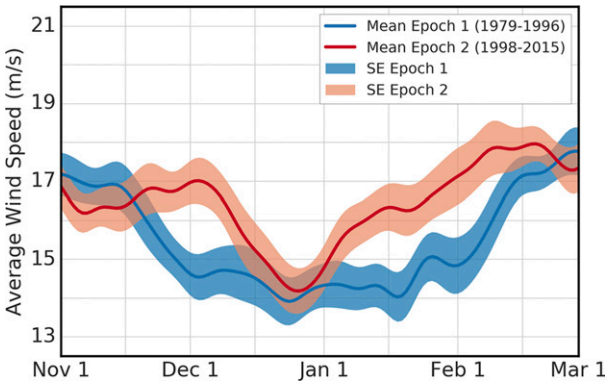

FIG. 11. Mean value for $\langle [u] \rangle$ ($\mathrm{m\,s^{-1}}$) as a function of day of the year, averaged across 50°–60°S, for the years 1979–96 (blue solid line) and 1998–2015 (red solid line). Shading indicates ±1 standard error interval for each set of years. Data are smoothed using a Gaussian window with a 7-day half width prior to calculation of statistics.

work are those changes that emerge around the 1 December period; the difference between the long-term means for the ozone depletion and recovery eras is particularly striking for this period. Based on our analysis in section 3, we propose that these apparent changes can be interpreted as a delayed equatorward transition of the jet, as a result of a long-term trend in the vortex breakdown date associated with ozone depletion (e.g., Thompson et al. 2011), rather than the more common interpretation of a poleward shift of the jet. Late breakdown years are associated with positive tropospheric circulation anomalies in the lead-up to the breakdown date (see Figs. 5b,d), and any trend toward later breakdown dates will therefore be associated with a trend toward positive tropospheric circulation anomalies. This behavior is illustrated in an idealized setting in Fig. 7d. In this schematic, for a year where the vortex breakdown date occurs approximately two weeks later than the climatological breakdown date, positive anomalies are seen to emerge on the poleward flank of the jet, centered around the time of the climatological vortex breakdown date. The circulation anomalies are subsequently seen to disappear following the seasonal transition of the jet. This highlights how a long-term delay in the seasonal transition will show up as an apparent poleward shift of the circulation, even though the physical interpretation is of course quite different.

The second apparent component to high-latitude trends is associated with changes to the mid-to-late summer circulation. From inspection of Fig. 10, it appears that in years with large ozone depletion the jet remains in its summer configuration for a reduced period of time and that it transitions poleward into its autumn profile at an earlier date. Previous work (e.g., Neff 1999; Sun et al. 2014) has linked changes in the tropospheric summer circulation with changes to the evolution of the stratospheric vortex breakdown process. In that respect it is worth noting that extreme late breakdown years, which occur preferentially in the later part of the record (Fig. 3), are associated with positive high-latitude zonal-wind anomalies at positive lags of 10–30 days (Fig. 5b), which would reach into January. Thus, these two features that are not accounted for by our schematic may in fact be linked. However, the period from mid-January onward is outside the scope of the present work, and so we do not attempt to explore these features further.

c. *High-latitude ENSO teleconnection in austral summer*

A prominent teleconnection that has been documented for the zonal-mean circulation is that between ENSO and the SH midlatitude jet during austral summer (Fig. 12a; see shaded region near 60°S during November and December in particular). This teleconnection has previously been interpreted as a direct response of the jet to tropical forcing; its seasonality has been argued to arise from a seasonally varying waveguide effect (Seager et al. 2003; L'Heureux and Thompson 2006). Here, we instead hypothesize that this teleconnection may be interpreted as the result of a correlation between the strength of the stratospheric vortex and the phase of ENSO and that its seasonality occurs as a result of the timing of the vortex breakdown (i.e., between November and January).

As a preliminary step in testing our hypothesis we note that the measure used for the zonal-mean circulation in Fig. 12a is interchangeable with $\langle [u] \rangle$ for the months November through February—the time series of monthly mean $[u]$ at 300 hPa has an interannual correlation >0.98 with monthly mean $\langle [u] \rangle$, across 50°–60°S, for each of the months November through February. This allows us to use our earlier results to interpret the high-latitude features of Fig. 12a. We next note that during the satellite era, 9 out of 12 El Niño episodes have been associated with early vortex breakdown years and 6 out of 10 La Niña episodes have been associated with late vortex breakdown years.[3] This would appear to be an unusually close association between the strength of the vortex and the phase of ENSO; we have made an attempt at quantifying this statement further in appendix B, where we provide evidence for an

[3] We associate each ENSO episode with the breakdown event that occurred during the episode. For example, the large El Niño episode of 1982/83 is associated with the (early) breakdown event of 1982.

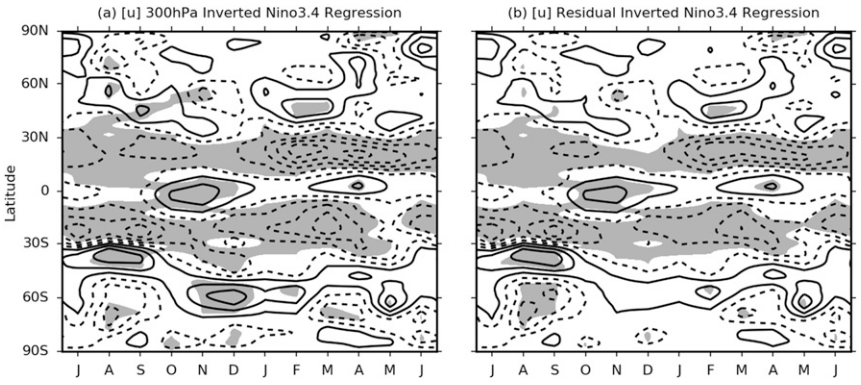

FIG. 12. (a) Monthly mean 300-hPa [u] anomalies and (b) monthly mean 300-hPa [u] residual anomalies regressed onto inverted values of the Niño-3.4 index. Residual time series formed by using the regression model in appendix A to remove the linear influence of the vortex breakdown event at each spatial point. Values of the Niño-3.4 index have been standardized and detrended prior to regression. Contour interval is 0.5 m s^{-1} (starting at ±0.25 m s^{-1}). Shading denotes relationships that are significant at the 5% level, based on the one-sided one-sample Student's t test for a reference mean value of zero. [(a) is adapted from Fig. 1 of L'Heureux and Thompson (2006).]

apparent statistical relationship between these two quantities. Next, we highlight the summer of 2015/16 as a year where the relationship between ENSO and jet latitude appeared to fail (L'Heureux et al. 2017); this summer was also anomalous in the sense that an El Niño occurred in association with a late breakdown of the vortex. The structure of the jet anomalies for this summer was relatively well explained by our anomaly composites for late breakdown years but was in opposition to that expected from Fig. 12a. This is despite 2015 being one of the strongest El Niño episodes on record (e.g., L'Heureux et al. 2017). Finally, we have repeated the regression analysis used to produce Fig. 12a using a residual time series formed by removing a regression model similar to appendix A. The high-latitude teleconnection is seen to vanish when the linear influence of the vortex breakdown event is accounted for (Fig. 12b).

We therefore argue that a parsimonious interpretation of the observed ENSO/midlatitude jet teleconnection during austral late spring–early summer is a correlation between the strength of the stratospheric vortex and the phase of ENSO. The organizing influence of the vortex breakdown on the tropospheric jet subsequently leads to a correlation between the phase of ENSO and the latitude of the jet. We acknowledge that this interpretation is somewhat speculative for the behavior suggested by the January and February regression values (i.e., these months are somewhat outside the scope of our results in section 3). However, we note that the apparent tendency for circulation anomalies to persist beyond the breakdown date in very late breakdown years offers a plausible explanation as to why regression values might persist weakly until February.

5. Summary and discussion

We have proposed that during SH late spring and early summer, high-latitude circulation variability is more usefully viewed as variability in the seasonal transition, which is organized around the date of the stratospheric vortex breakdown, rather than as anomalies to a climatological seasonal cycle. We have subsequently explored the implications of this perspective for previous results in the literature. We argue that there are at least four clear examples where this perspective appears to shed new light.

First, we have illustrated how anomaly composites must be interpreted with care when statistical models of circulation variability exhibit nonstationary behavior. We have used our proposed perspective on circulation variability to offer a different interpretation of the anomaly composites that were originally introduced by Black and McDaniel (2007) and find a much stronger relationship between vortex breakdown and tropospheric circulation than they did. This interpretation is argued to be consistent with the more recent results of Sun et al. (2014).

Second, we have presented evidence that the SH high-latitude ENSO teleconnection can be interpreted as a correlation between the phase of ENSO and the strength of the stratospheric vortex, rather than as a direct effect from the tropics. According to this hypothesis, the organizing influence of the vortex breakdown on the high-latitude circulation would then lead to the emergence of this teleconnection in SH late spring–summer. An important caveat attached to our analysis is that we have only considered zonal-mean teleconnections; traditionally, it is the zonal asymmetries

that have been the focus of teleconnection studies. Our results make no conclusions about high-latitude teleconnections associated with the SH zonally asymmetric circulation. However, we caution that in the absence of a greater understanding of (for example) midlatitude stratosphere–troposphere coupling mechanisms, the causal nature of any such teleconnections should be treated with care. Furthermore, if robust, the correlation between the phase of ENSO and the strength of the SH stratospheric vortex warrants further attention as to the precise nature of this relationship.

Third, we have argued that the increased SAM time scales encompassing late spring and summer can be viewed as reflecting variability in the timing of the seasonal transition, rather than as weakened damping of SAM anomalies by eddy feedbacks. This increase in SAM time scales has often been interpreted as a potential time of year where long-range forecast skill may be possible (see Kidston et al. 2015, and references therein). Our interpretation is consistent with this suggestion, although for different reasons than generally believed. In particular, our proposed interpretation of the ''source'' of these increased time scales (variability in the date of the breakdown of the stratospheric vortex) suggests that long-range forecast skill associated with the stratospheric vortex should also lead to a realization of long-range forecast skill in the prediction of the latitude of the tropospheric jet; the recent results of Seviour et al. (2014) offer some promise in this respect. However, it should also be acknowledged that there is still much to be improved in the current generation of climate models (Wilcox and Charlton-Perez 2013); the diagnostic used in this study $\langle [u] \rangle$ may represent a helpful tool for assessing model fidelity. It is unclear how instructive, if at all, our results may be for improving understanding of the increased time scales of the northern annular mode (NAM) in boreal winter (Baldwin et al. 2003).

Fourth, we have presented evidence that SH high-latitude climate change can be separated into at least two distinct time periods and that for the earliest of these time periods (December), changes are more physically interpreted as a delayed equatorward transition of the jet, rather than a poleward shift. From inspection of the anomaly patterns at positive lags for extreme late breakdown years, which occur preferentially in the later part of the record, it would appear that a deeper understanding of the dynamics of this transition may also be beneficial for an improved understanding of changes in the later time period (January–February).

Understanding why the jet transitions equatorward in association with the breakdown of the stratospheric vortex is perhaps the outstanding question that emerges from the present study. That the stratospheric vortex can exert a persistent influence on the tropospheric jet appears to be a characteristic feature across a wide range of models (e.g., Sun et al. 2014); furthermore, it would appear that the tropospheric jet can shift seasonally even when the only imposed seasonality is in the stratosphere (e.g., Sun and Robinson 2009; Sheshadri et al. 2015). To understand this behavior further, it would appear pertinent to revisit theories for the maintenance of the westerlies and what ''sets'' the latitude of the jet.

In the absence of a complete theory for jet latitude, the concept of a circulation regime (e.g., Palmer 1999) may offer a complementary perspective for predicting the SH circulation response to external forcing (e.g., anthropogenic forcing). In the present paper we have argued that the response of the SH zonal-mean circulation to external forcing (ozone depletion) may be partly interpreted as an increased residency time in the spring regime, consistent with the results of Lee and Feldstein (2013). Recent work (Ivy et al. 2017) has documented apparent long-term changes to the SH jet in May, which share qualitative similarities with changes to the jet in austral spring–summer. May is notable as the climatological month where the zonal-mean SH circulation transitions to a winter regime (e.g., Neff 1999), hinting that SH circulation responses to external forcing may emerge most clearly around the time of a seasonal (regime) transition. Whether or not such a perspective offers a helpful reformulation of the SH jet changes in May is unclear at the present time.

Finally, we argue that the combined evidence of these four examples demonstrates that the traditional paradigm of decomposing circulation variability into anomalies about a long-term climatological seasonal cycle may not always be the optimal approach; such a decomposition is perhaps traditionally motivated by analogy with linearized perturbations to a ''basic state,'' with the implicit assumption of a time-scale separation. In the four examples outlined above, we have shown how a nonstationary model of circulation variability, which incorporates a deterministic representation of the organizing influence of the vortex breakdown, represents a simpler means of viewing circulation variability [see also Koutsoyiannis (2011) for a discussion on the correspondence between nonstationary processes and deterministic behavior]. Furthermore, the concept of a basic state may have limited physical meaning in this nonstationary model of circulation variability. Such nonstationary models of circulation variability need not be restricted to intraseasonal time scales: recent work (Byrne et al. 2016) has highlighted a pronounced quasi-2-yr time scale to

SH high-latitude circulation variability, which is most likely linked to stratospheric processes. This suggests that the organizing influence of the vortex can lead to high-latitude tropospheric circulation variability on both the intraseasonal and the interannual time scales.

The concept of an organizing influence of the vortex breakdown (Black et al. 2006; Black and McDaniel 2007) appears to be a powerful paradigm within which to interpret high-latitude tropospheric variability. It has previously been applied to the NH circulation, within a framework that models variability as (statistically stationary) anomalies to a long-term climatological seasonal cycle (Black et al. 2006). The results of the present work suggest that it may be of benefit to revisit the results of this study, within a modeling framework of nonstationary variability. Related applications that may likewise benefit from the perspective of circulation variability proposed in this paper include, but are not limited to, detection and attribution methodologies that are restricted by large internal variability at high latitudes, the assessment of forecast skill in the presence of an artificial climatology (e.g., Hamill and Juras 2006), and the use of statistical tests that treat the population parameters as fixed in time.

Acknowledgments. We thank Andrew Charlton-Perez, Tom Frame, and Giuseppe Zappa for helpful discussions and suggestions and two anonymous reviewers for their constructive comments. Funding support is acknowledged from the European Union's F7 research and innovation program under the Marie Skodowska-Curie Grant Agreement 654492 and from European Research Council Advanced Grant "Understanding the Atmospheric Circulation Response to Climate Change" (ACRCC), Project 339390. Part of the work was done during an extended visit by RAP to the University of Reading, with support provided by the Department of Meteorology Visitors Programme. We thank the European Centre for Medium-Range Weather Forecasts for the ERA-Interim data, NASA Goddard Space Flight Center Atmospheric Chemistry and Dynamics Laboratory for the EESC data, and NOAA/Earth System Research Laboratory for the ENSO data.

APPENDIX A

Linear Statistical Model

As an attempt at quantifying the organizing influence of the breakdown of the stratospheric vortex on the variability of the tropospheric jet, we construct a linear statistical model between the vortex breakdown date and the November–December (ND) mean of daily tropospheric jet latitude, following the procedures outlined in Wilks (2011). We denote our time series for vortex breakdown date $x(t)$ and our time series for ND jet latitude $y(t)$. We have 37 data points for each index and prior to construction of our statistical model we linearly detrend each index. The statistical model is given by

$$y(t) = \beta x(t) + \varepsilon(t),$$

where β represents the regression coefficient estimated using an ordinary least squares method and $\varepsilon(t)$ is a residual error. For our entire dataset we find a correlation value of $r \approx 0.73$ and a regression coefficient of $\beta(t) \approx 0.14°\,\text{latitude day}^{-1}$ (i.e., a delay of one week in the breakdown date is associated with an increase of 1° in ND jet latitude). We have confirmed the robustness of this relationship by repeating the procedure for only the first half and only the second half of our dataset and for only the early breakdown years and only the late breakdown years, as well as by employing a leave-one-out method. We have also checked for any possible nonlinearity in the relationship by inspection of a scatterplot and have analyzed a box plot and a quantile–quantile (q-q) plot to confirm that the residual appears to be normally distributed.

APPENDIX B

Relationship between ENSO Phase and Vortex Strength

There have been 12 El Niño (EN) and 10 La Niña (LN) episodes during the satellite era (see data and methods section for how we define the phase of ENSO). Nine EN episodes have been associated with early breakdown (E) years and six LN episodes have been associated with late breakdown (L) years. For brevity, we introduce the notation (9, 6) to represent this combination. We are interested in quantifying how likely it is that at least nine EN episodes occur in association with E years as well as at least six LN episodes in association with L years. For the purposes of this calculation, we consider the year associated with the median breakdown date (1993) as an E year. Our conclusions do not change if we instead classify it as an L year.

First we note that there are $\binom{37}{12} \times \binom{25}{10}$ possible ways of distributing EN and LN episodes among the 37 yr of our satellite record. Next we note that we require at least nine EN episodes to occur in E years

$\left[\binom{19}{9}\right]$ and at least six LN episodes to occur in L years $\left[\binom{18}{6}\right]$. We now consider all possible combinations that satisfy this criterion and calculate the number of ways of selecting each combination. For example, (10, 8) represents a valid combination; there are $\binom{19}{10} \times \binom{18}{8} \times \binom{10}{2} \times \binom{9}{2}$ ways of selecting this combination. Code has been written that sums the number of ways of selecting each of the 20 possible valid combinations (x, y) and subsequently computes the ratio of this sum to $\binom{37}{12} \times \binom{25}{10}$. This ratio is found to be 0.034; that is, the relationship between ENSO phase and vortex strength is found to be statistically significant at the 5% level, according to our measures of ENSO phase and vortex strength.

REFERENCES

Anstey, J. A., and T. G. Shepherd, 2014: High-latitude influence of the quasi-biennial oscillation. *Quart. J. Roy. Meteor. Soc.*, **140**, 1–21, doi:10.1002/qj.2132.

Baldwin, M. P., D. B. Stephenson, D. W. J. Thompson, T. J. Dunkerton, A. J. Charlton, and A. O'Neill, 2003: Stratospheric memory and skill of extended-range weather forecasts. *Science*, **301**, 636–640, doi:10.1126/science.1087143.

Black, R. X., and B. A. McDaniel, 2007: Interannual variability in the Southern Hemisphere circulation organized by stratospheric final warming events. *J. Atmos. Sci.*, **64**, 2968–2974, doi:10.1175/JAS3979.1.

——, ——, and W. A. Robinson, 2006: Stratosphere–troposphere coupling during spring onset. *J. Climate*, **19**, 4891–4901, doi:10.1175/JCLI3907.1.

Byrne, N. J., T. G. Shepherd, T. Woollings, and R. A. Plumb, 2016: Annular modes and apparent eddy feedbacks in the Southern Hemisphere. *Geophys. Res. Lett.*, **43**, 3897–3902, doi:10.1002/2016GL068851.

Dee, D. P., and Coauthors, 2011: The ERA-Interim reanalysis: Configuration and performance of the data assimilation system. *Quart. J. Roy. Meteor. Soc.*, **137**, 553–597, doi:10.1002/qj.828.

Fogt, R. L., J. Perlwitz, A. J. Monaghan, D. H. Bromwich, J. M. Jones, and G. J. Marshall, 2009: Historical SAM variability. Part II: Twentieth-century variability and trends from reconstructions, observations, and the IPCC AR4 models. *J. Climate*, **22**, 5346–5365, doi:10.1175/2009JCLI2786.1.

Gerber, E. P., and Coauthors, 2010: Stratosphere-troposphere coupling and annular mode variability in chemistry-climate models. *J. Geophys. Res.*, **115**, D00M06, doi:10.1029/2009JD013770.

Hamill, T. M., and J. Juras, 2006: Measuring forecast skill: Is it real skill or is it the varying climatology? *Quart. J. Roy. Meteor. Soc.*, **132**, 2905–2923, doi:10.1256/qj.06.25.

Hartmann, D. L., and F. Lo, 1998: Wave-driven zonal flow vacillation in the Southern Hemisphere. *J. Atmos. Sci.*, **55**, 1303–1315, doi:10.1175/1520-0469(1998)055<1303:WDZFVI>2.0.CO;2.

IPCC, 2013: *Climate Change 2013: The Physical Science Basis.* Cambridge University Press, 1535 pp., doi:10.1017/CBO9781107415324.

Ivy, D. J., C. Hilgenbrink, D. Kinnison, R. A. Plumb, A. Sheshadri, S. Solomon, and D. W. J. Thompson, 2017: Observed changes in the Southern Hemispheric circulation in May. *J. Climate*, **30**, 527–536, doi:10.1175/JCLI-D-16-0394.1.

Kidston, J., A. A. Scaife, S. C. Hardiman, D. M. Mitchell, N. Butchart, M. P. Baldwin, and L. J. Gray, 2015: Stratospheric influence on tropospheric jet streams, storm tracks and surface weather. *Nat. Geosci.*, **8**, 433–440, doi:10.1038/ngeo2424.

Kim, J., and T. Reichler, 2016: Quantifying the uncertainty of the annular mode time scale and the role of the stratosphere. *Climate Dyn.*, **47**, 637–649, doi:10.1007/s00382-015-2860-2.

Koutsoyiannis, D., 2011: Hurst-Kolmogorov dynamics and uncertainty. *J. Amer. Water Resour. Assoc.*, **47**, 481–495, doi:10.1111/j.1752-1688.2011.00543.x.

Lee, S., and S. B. Feldstein, 2013: Detecting ozone- and greenhouse gas–driven wind trends with observational data. *Science*, **339**, 563–567, doi:10.1126/science.1225154.

L'Heureux, M. L., and D. W. J. Thompson, 2006: Observed relationships between the El Niño–Southern Oscillation and the extratropical zonal-mean circulation. *J. Climate*, **19**, 276–287, doi:10.1175/JCLI3617.1.

——, and Coauthors, 2017: Observing and predicting the 2015–16 El Niño. *Bull. Amer. Meteor. Soc.*, doi:10.1175/BAMS-D-16-0009.1, in press.

McIntyre, M. E., 2015: Balanced flow. *Encyclopedia of Atmospheric Sciences*, 2nd ed. G. R. North, J. Pyle, and F. Zhang, Eds., Academic Press, 298–303, doi:10.1016//B978-0-12-382225-3.00484-9.

Mudryk, L. R., and P. J. Kushner, 2011: A method to diagnose sources of annular mode time scales. *J. Geophys. Res.*, **116**, D14114, doi:10.1029/2010JD015291.

Neff, W. D., 1999: Decadal time scale trends and variability in the tropospheric circulation over the South Pole. *J. Geophys. Res.*, **104**, 27 217–27 251, doi:10.1029/1999JD900483.

Newman, P. A., E. R. Nash, S. R. Kawa, S. A. Montzka, and S. M. Schauffler, 2006: When will the Antarctic ozone hole recover? *Geophys. Res. Lett.*, **33**, L12814, doi:10.1029/2005GL025232.

North, G. R., T. L. Bell, R. F. Cahalan, and F. J. Moeng, 1982: Sampling errors in the estimation of empirical orthogonal functions. *Mon. Wea. Rev.*, **110**, 699–706, doi:10.1175/1520-0493(1982)110<0699:SEITEO>2.0.CO;2.

Palmer, T. N., 1999: A nonlinear dynamical perspective on climate prediction. *J. Climate*, **12**, 575–591, doi:10.1175/1520-0442(1999)012<0575:ANDPOC>2.0.CO;2.

Seager, R., N. Harnik, Y. Kushnir, W. A. Robinson, and J. Miller, 2003: Mechanisms of hemispherically symmetric climate variability. *J. Climate*, **16**, 2960–2978, doi:10.1175/1520-0442(2003)016<2960:MOHSCV>2.0.CO;2.

Seviour, W. J. M., S. C. Hardiman, L. J. Gray, N. Butchart, C. MacLachlan, and A. A. Scaife, 2014: Skillful seasonal prediction of the southern annular mode and Antarctic ozone. *J. Climate*, **27**, 7462–7474, doi:10.1175/JCLI-D-14-00264.1.

Sheshadri, A., R. A. Plumb, and E. P. Gerber, 2015: Seasonal variability of the polar stratospheric vortex in an idealized AGCM with varying tropospheric wave forcing. *J. Atmos. Sci.*, **72**, 2248–2266, doi:10.1175/JAS-D-14-0191.1.

Simpson, I. R., P. Hitchcock, T. G. Shepherd, and J. F. Scinocca, 2011: Stratospheric variability and tropospheric annular-mode timescales. *Geophys. Res. Lett.*, **38**, L20806, doi:10.1029/2011GL049304.

Solomon, S., D. J. Ivy, D. Kinnison, M. J. Mills, R. R. Neely, and A. Schmidt, 2016: Emergence of healing in the Antarctic ozone layer. *Science*, **310**, 307–310, doi:10.1126/science.aae0061.

Sun, L., and W. A. Robinson, 2009: Downward influence of stratospheric final warming events in an idealized model. *Geophys. Res. Lett.*, **36**, L03819, doi:10.1029/2008GL036624.

——, G. Chen, and W. A. Robinson, 2014: The role of stratospheric polar vortex breakdown in Southern Hemisphere climate trends. *J. Atmos. Sci.*, **71**, 2335–2353, doi:10.1175/JAS-D-13-0290.1.

Thompson, D. W. J., and J. M. Wallace, 2000: Annular modes in the extratropical circulation. Part I: Month-to-month variability. *J. Climate*, **13**, 1000–1016, doi:10.1175/1520-0442(2000)013<1000:AMITEC>2.0.CO;2.

——, M. P. Baldwin, and S. Solomon, 2005: Stratosphere–troposphere coupling in the Southern Hemisphere. *J. Atmos. Sci.*, **62**, 708–715, doi:10.1175/JAS-3321.1.

——, S. Solomon, P. J. Kushner, M. H. England, K. M. Grise, and D. J. Karoly, 2011: Signatures of the Antarctic ozone hole in Southern Hemisphere surface climate change. *Nat. Geosci.*, **4**, 741–749, doi:10.1038/ngeo1296.

Wilcox, L. J., and A. J. Charlton-Perez, 2013: Final warming of the Southern Hemisphere polar vortex in high- and low-top CMIP5 models. *J. Geophys. Res. Atmos.*, **118**, 2535–2546, doi:10.1002/jgrd.50254.

Wilks, D. S., 2011: *Statistical Methods in the Atmospheric Sciences.* 3rd ed. Academic Press, 676 pp., doi:10.1016/B978-0-12-385022-5.00022-1.